Waveguides in inverted opal photonic crystals

Virginie Lousse [1,2] **and Shanhui Fan** [1]

[1] *Ginzton Laboratory, Stanford University, Stanford, California 94305, USA*
[2] *Laboratoire de Physique du Solide, Facultés Universitaires Notre-Dame de la Paix, B-5000 Namur, Belgium*

virginie.lousse@stanford.edu

Abstract: Waveguiding phenomena are investigated in an inverted opal photonic crystal made of interpenetrating air spheres, coated with amorphous Ge. Here we focus on the complete gap between the 8th and the 9th band, since a projected band analysis reveals that it is difficult to use the large lower incomplete gap for guiding purposes. Two kinds of line defects are analyzed within this photonic structure, with the plane-wave expansion method. The first one consists of an air cylinder in the $\Gamma - K$ direction. It gives rise to a large number of defect modes in the bandgap. Most of these modes have large field components at the surface. The second defect is an array of air spheres, also along the $\Gamma - K$ direction. This is shown to avoid the surface-like modes and sustain only two modes associated with different polarizations, in the frequency range of interest. The air mode waveguiding bandwidth reaches up to 113 nm centered at a wavelength of $1.5\mu m$.

OCIS codes: (130.2790) Guided waves; (160.3130) Integrated optics materials.

References and links

1. K. Ohtaka, and M. Inoue, "Light scattering from macroscopic spherical bodies," Phys. Rev. B **25**, 677 (1982).
2. E. Yablonovitch, "Inhibited Spontaneous Emission in Solid-State Physics and Electronics," Phys. Rev. Lett. **58**, 2059 (1987).
3. S. John, "Strong localization of photons in certain disordered dielectric superlattices," Phys. Rev. Lett. **58**, 2486 (1987).
4. A. Mekis, J.C. Chen, I. Kurland, S. Fan, P.R. Villeneuve, and J.D. Joannopoulos, "High transmission through sharp bends in photonic crystals waveguides," Phys. Rev. Lett. **77**, 3787 (1996).
5. S.-Y. Lin, E. Chow, V. Hietala, P.R. Villeneuve, and J.D. Joannopoulos, "Experimental demonstration of guiding and bending of electromagnetic waves in a photonic crystal," Science **282**, 274 (1998).
6. A. Chutinan, and S. Noda, "Highly confined waveguides and waveguide bends in three-dimensional photonic crystal," Appl. Phys. Lett. **75**, 3739 (1999).
7. S. Noda, K. Tomoda, N. Yamamoto, and A. Chutinan, "Full three-dimensional photonic bandgap crystals at near-infrared wavelengths," Science **289**, 604 (2000).
8. C. Sell, C. Christensen, J. Muehlmeier, G. Tuttle, Z.Y. Li, and K.M. Ho, "Waveguide networks in three-dimensional layer-by-layer photonic crystals," Appl. Phys. Lett. **84**, 4605 (2004).
9. Z.Y. Li and K.M. Ho, "Waveguides in three-dimensional layer-by-layer photonic crystals," J. Opt. Soc. Am. B **20**, 801 (2003).
10. M.L. Povinelli, S.G. Johnson, S. Fan, and J.D. Joannopoulos, "Emulation of two-dimensional photonic crystal defect modes in a photonic crystal with a three-dimensional photonic band gap," Phys. Rev. B **64**, 075,313 (2001).
11. A. Chutinan, and S. John, "Diffractionless flow of light in two- and three-dimensional photonic band gap heterostructures: Theory, design rules, and simulations," Phys. Rev. E **71**, 026,605 (2005).
12. V.N. Astratov, et al, "Optical spectroscopy of opal matrices with CdS embedded in its pores: quantum confinement and photonic bandgap effects." Nuovo Cimento D **17**, 1349 (1995).

#9476 - $15.00 USD Received 15 November 2005; revised 5 November 2005; accepted 11 November 2005

13. J. Wijnhoven, and W. Vos, "Preparation of photonic crystals made of air spheres in titania," Science **281**, 802 (1998).
14. Y.A. Vlasov, N. Yao, and D.J. Norris, "Synthesis of photonic crystals for optical wavelengths from semiconductor quantum dots." Adv. Mater. **11**, 165 (1999).
15. P.V. Braun, and P. Wiltzius, "Electrochemically grown photonic crystals," Nature **402**, 603 (1999).
16. M. Muller, R. Zentel, T. Maka, S.G. Romanov, and C.M. Sotomayor-Torres, "Photonic crystal films with high refractive index contrast," Adv. Mater. **12**, 1499 (2000).
17. A. Blanco, et al, "Large-scale synthesis of a silicon photonic crystal with a complete three-dimensional bandgap near 1.5 micrometres," Nature **405**, 437 (2000).
18. Y.A. Vlasov, X.-Z. Bo, J.C. Sturm, and D.J. Norris, "On-chip natural assembly of silicon photonic bandgap crystals," Nature **414**, 289 (2001).
19. F. Garcia-Santamaria, M. Ibisate, I. Rodriguez, F. Meseguer, and C. Lopez, "Photonic band engineering in opals by growth of Si/Ge multilayer shells," Adv. Mater. **15**, 788 (2003).
20. W. Lee, S.A. Pruzinsky, and P.V. Braun, "Multi-photon polymerization of waveguide structures within three-dimensional photonic crystals," Adv. Mater. **14**, 271 (2002).
21. S.G. Johnson, and J.D. Joannopoulos, "Block-iterative frequency-domain methods for Maxwell's equations in a planewave basis," Opt. Express **8**, 173 (2001), http://www.opticsexpress.org/abstract.cfm?URI=OPEX-8-3-173.
22. J.D. Joannopoulos, R.D. Meade, and J.N. Winn, *Photonic Crystals, Molding the Flow of Light.* (Princeton University Press, Princeton, New Jersey, 1995).
23. W.T. Lau, and S. Fan, "Creating large bandwidth line defects by embedding dielectric waveguides into photonic crystal slabs," Appl. Phys. Lett. **81**, 3915 (2002).
24. H.K. Kim, J. Shin, S. Fan, M.J.F. Digonnet, and G.S. Kino, "Designing air-core photonic-bandgap fibers free of surface modes," IEEE J. Quantum Electron. **40**, 551 (2004).
25. A. Yariv, Y. Xu, R.K. Lee, and A. Scherer, "Coupled-resonator optical waveguide: a proposal and analysis," Opt. Lett. **24**, 711 (1999).
26. V. Yannopapas, A. Modinos, and N. Stefanou, "Waveguides of defect chains in photonic crystals," Phys. Rev. B **65**, 235201 (2002).
27. Z.Y. Li, and Z.Q. Zhang, "Fragility of photonic band gaps in inverse-opal photonic crystals," Phys. Rev. B **62**, 1516 (2000).

1. Introduction

Photonic crystals (PC) are periodic dielectric structures [1] which may forbid the propagation of the electromagnetic waves in a certain frequency range [2-3]. A unique feature of a waveguide structure in a photonic crystal is its ability to guide light in air. In the last few years, theoretical and experimental studies have shown that line defects with air in two-dimensional (2D) dielectric photonic bandgap (PBG) structures can be used as efficient waveguides for frequencies within the in-plane bandgap [4-5]. However, the electromagnetic waves are not confined in the direction perpendicular to the plane. This leads to intrinsic radiation loss in the third dimension. A solution to avoid this out-of-plane radiation is to consider air waveguides in three-dimensional (3D) PBG materials [6-11]. In particular, air waveguides in lithographically defined photonic crystals have been considered in [6-10].

In contrast to lithographical techniques, self-assembly methods have been explored as a simple and inexpensive way to make 3D PBG materials [12-17]. The sample quality of these colloidal crystals has dramatically improved in the last few years [18-19]. As a consequence, the use of these structures may open a route towards the realization of large-scale optical integrated circuits. Photonic bandgap based waveguides require the incorporation of a line defect within the 3D structure. Previously, a line defect structure in a 2D slab sandwiched between two opal structures has been considered by Chutinan and John. Such a structure, however, requires an accurate alignment between two 3D structures.

Recently, a multi-photon polymerization technique, with the use of a laser confocal microscope, has been successfully demonstrated as a pathway for pattern generation within colloidal assemblies [20]. This method enables one to create a line defect after the opal structure has been defined, and thus provides great flexibility in constructing integrated photonic circuits. To our knowledge, no systematic theoretical studies on the properties of these waveguides have

#9476 - $15.00 USD Received 15 November 2005; revised 5 November 2005; accepted 11 November 2005

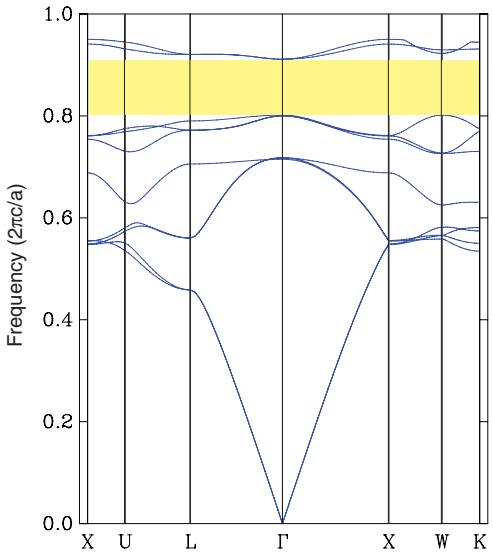

Fig. 1. Band structure of interpenetrating air spheres coated with amorphous Ge (n=4.1) in a fcc lattice. The radius of the air spheres is 0.3645a and the external radius of the semiconductor shell is 0.409a. A complete bandgap of 12.8%, marked by a yellow region, exists between the 8^{th} and 9^{th} bands.

been published yet. In this paper, we calculate the bandstructures of these inverse opals photonic crystals containing linear air defects. Several waveguides geometries are considered and the air mode waveguiding bandwidth is optimized.

2. Inverted opals band structure

The structure considered in this work is made of interpenetrating air spheres coated with amorphous Ge (n=4.1) in a fcc lattice [19]. The radius of the air spheres is 0.3645a and the external radius of the semiconductor shell is 0.409a, where a is the lattice constant. The volume fraction of dielectric materials is approximately 16%. The band diagram of this inverted opal photonic crystal can be found in Fig. 1. Of particular interest for our work is the complete bandgap between the 8^{th} and 9^{th} bands.

The structure also presents a wide stop band in the $\Gamma - L$ direction, between the 2^{nd} and the 3^{rd} band, in the normalized frequency range $a/\lambda = 0.46 - 0.56$. The size of this stop band is $\sim 20\%$ when measured as a percentage of the center frequency. Reflection using this stop band has been extensively probed experimentally. We have found however that it is difficult to use this incomplete gap for waveguiding purposes. The reason is as follows. Writing a waveguide which could optimally use the mirror effect of this gap would require defining a guiding direction perpendicular to the $\Gamma - L$ direction. A highly symmetric example is the $\Gamma - K$ direction, along $[1\bar{1}0]$. We define this direction as the z direction. In order to create a guided mode with a particular k_z, the structure needs to have a complete gap at that particular k_z point. We therefore project the entire band diagram onto the $\omega - k_z$ plane. Figure 2 shows the projected band structure of the infinite crystal along the $\Gamma - K$ direction. The shaded regions correspond to the frequencies of propagating electromagnetic modes in the inverse opal structure. This figure clearly shows that there is no transverse bandgap between the 2^{nd} and the 3^{rd} band for the $\Gamma - K$ direction. The same negative result has in fact been reached for all high-symmetry directions of this fcc structure in this range of frequencies. As an example, the projected band diagram along

#9476 - $15.00 USD Received 15 November 2005; revised 5 November 2005; accepted 11 November 2005

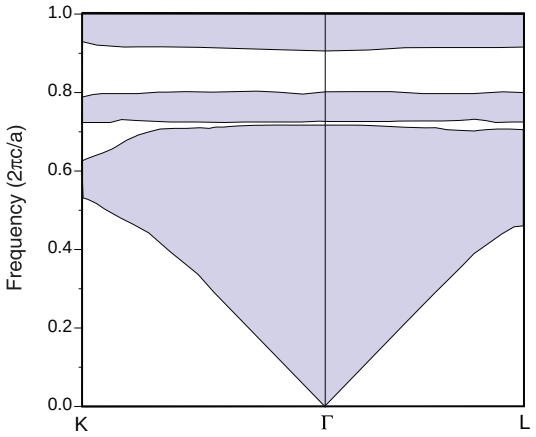

Fig. 2. Projected band structure of the infinite crystal along the $\Gamma - K$ and $\Gamma - L$ directions in the Brillouin zone. The K point is located at a distance $(\frac{3\sqrt{2}}{4})(\frac{2\pi}{a})$ away from Γ along $[0\bar{1}1]$. The L point is located at a distance $(\frac{\sqrt{3}}{2})(\frac{2\pi}{a})$ away from Γ along $[111]$. The shaded regions correspond to the propagating electromagnetic modes in the inverse opal structure.

the $\Gamma - L$ direction is also shown in Fig. 2. Thus, the gap between the 2^{nd} and the 3^{rd} band cannot be exploited to propagate light through a line defect, whatever the direction chosen for the waveguide.

In order to guide light in an inverted opal photonic crystal, it is therefore necessary to use the large complete bandgap of 12.8% between the 8^{th} and 9^{th} bands, in the normalized frequency range $a/\lambda = 0.80 - 0.91$. Experimentally, in the two-photon polymerisation technique, writing waveguides is easiest in any of the directions in the (111) plane, and one of these is the $\Gamma - K$ orientation. Thus, line defects in this direction are considered in this work.

3. Cylindrical waveguide

We first consider a cylindrical air waveguide introduced through the inverted opal structure. The guide is specifically oriented along the $\Gamma - K$ (i.e. $[1\bar{1}0]$) direction, named the z axis in the rest of this work. Its axis passes through the point $(\frac{1}{2},0,0)$ in a non-primitive unit cell defined by the orthogonal lattice vectors: $\vec{a_1}' = (\frac{a}{2},\frac{a}{2},0)$, $\vec{a_2}' = (0,0,a)$, $\vec{a_3}' = (\frac{a}{2},-\frac{a}{2},0)$, with the origin of the lattice vectors chosen to coincide with the center of a sphere in the opal structure. Therefore, in this non-primitive basis defining an orthorhombic lattice, the two elementary spheres defining the fcc structure are located at the points $(0,0,0)$ and $(\frac{1}{2},\frac{1}{2},\frac{1}{2})$.

Line-defects modes are analyzed with the plane-wave expansion method, where Maxwell's equations are solved in the frequency domain [21]. A supercell with the size $5\frac{\sqrt{2}}{2}a \times 5a \times 1\frac{\sqrt{2}}{2}a$, shown in Fig. 3, is used to calculate the dispersion relations of the waveguide modes and approximately 820 000 plane waves are used in the calculation. The projected bands corresponding to bulk modes are computed using a defect-free supercell. Each supercell contains 50 primitive unit cells. As a consequence, in the case of a perfect crystal, 400 bands appear below the photonic bandgap.

The band diagram for the waveguides are shown in Fig. 4. The frequency regions of propagating electromagnetic modes in the three-dimensional photonic crystal are represented as shaded blue regions on the projected band diagrams. The frequencies of these modes are plotted as a function of k_z, the component of the wavevector along the direction of the linear defect, which

#9476 - $15.00 USD Received 15 November 2005; revised 5 November 2005; accepted 11 November 2005

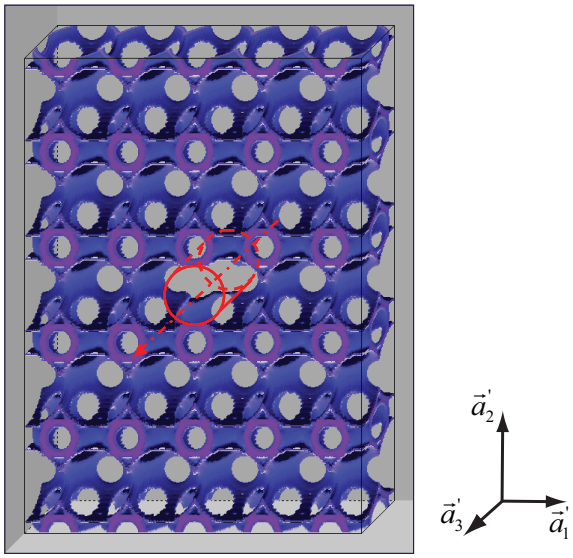

Fig. 3. Supercell used to calculate the dispersion relations of the waveguide modes. The size of the supercell is $5\frac{\sqrt{2}}{2}a \times 5a \times 1\frac{\sqrt{2}}{2}a$. The blue regions correspond to the Ge shells, which lie at the interstitial region between the air spheres of the inverted opal structure. A cylindrical waveguide of radius $R = 0.3a$ is located at the center of the supercell and is oriented along the $[1\bar{1}0]$ direction represented by the red arrow.

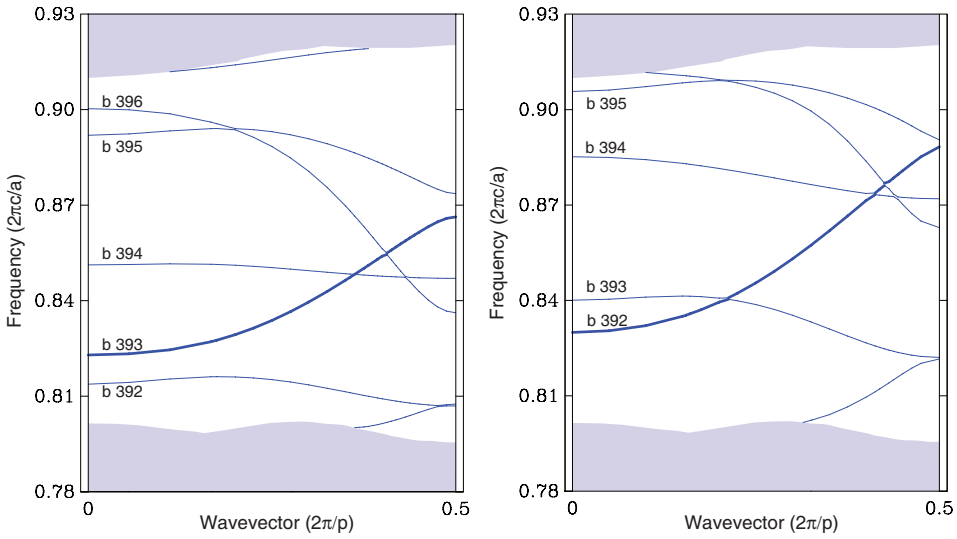

(a) $R = 0.25a$ (b) $R = 0.30a$

Fig. 4. Projected band structure for the inverse opal photonic crystal with a linear defect created by an air cylinder of radius R. The cylinder is along the $[1\bar{1}0]$ direction. The periodicity p in this direction is $\frac{\sqrt{2}}{2}\ a$. The shaded blue areas indicate the propagating modes in the perfect three-dimensional photonic crystal. The thick line indicates the band that possesses a significant fraction of energy in air.

#9476 - $15.00 USD Received 15 November 2005; revised 5 November 2005; accepted 11 November 2005

takes on values between 0 and π/p, where $p = \sqrt{2}a/2$. For waveguides of radius $R = 0.25\,a$ and $R = 0.30\,a$, the band diagrams are shown in Fig. 4(a) and (b), respectively. The choice of these particular radii for the waveguides is based on an analogy with a metallic waveguide. In a metallic waveguide, for a guided mode, the field must vanish exactly at the perfectly reflecting walls. We therefore chose the radius such that for a frequency inside the complete bandgap, approximately half a wavelength would fit between the walls. This produces a waveguide radius varying between $0.28\,a$ and $0.31\,a$. By perturbing the photonic crystal with the cylindrical waveguide, we push several bands into the omnidirectional gap between the 8^{th} and 9^{th} bands.

It is apparent in Fig. 4(b) that the waveguide of radius of $R = 0.30\,a$ provides a single mode (corresponding to the 392^{th} band) with a relatively large group velocity over a substantial region of $\Gamma - K$ wavevectors. However this band is intersected by a large number of very flat bands (e.g. band No. 393, 394, ...).(We note that the band numbers here are specific to our choice of the computational cell. We retain these numbers for the convenience of description.)

Figure 5 shows, for a cylindrical waveguide of radius $R = 0.30\,a$, the energy in the electric field at the Brillouin zone center for the bands labelled $392, 393, 394$ and 395, respectively. We plot the energy distribution on a plane perpendicular to the waveguide. The position of the plane is chosen such that the cross-section cuts through the location of maximal electric field intensities. The waveguide's circular cross-section can be seen at the center of each map. The defect modes are strongly localized near the defect. Only the mode in the band 392 has a significant fraction of energy inside the air region for every position of z. (As an additional example, the intensity plot on the plane $z = \sqrt{2}a/4$ is shown in Fig. 6.) For the bands 393, 394, and 395, the electric field energy is found to be mostly in the high dielectric regions, at the surface of the waveguide. These modes with large surface states components are undesirable as they are more susceptible to scattering loss in the presence of disorder.

The surface-like modes are also present in other cylindrical waveguide geometry we considered. For waveguides of radius $R = 0.30\,a$ with an axis passing through the point $(0,0,0)$ or through the point $(\frac{1}{4},\frac{1}{4},0)$ in the non-primitive unit cell, it has been observed that a larger number of bands arise in the photonic bandgap, compared to the case of a waveguide passing through the point $(\frac{1}{2},0,0)$ studied earlier.

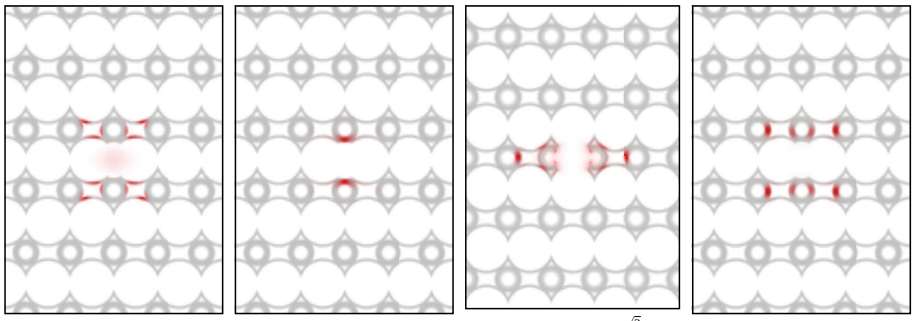

(a) band 392, $z = 0$ (b) band 393, $z = 0$ (c) band 394, $z = \frac{\sqrt{2}}{4}a$ (d) band 395, $z = 0$

Fig. 5. Energy in the electric field for the modes at the Brillouin zone center, in the defect bands inside the bandgap. The gray regions represent Ge. The defect consists of a cylindrical air waveguide of radius $R = 0.30\,a$ along the $[1\bar{1}0]$ direction. For each of these bands, the plot describes the electric energy distribution on the plane perpendicular to the waveguide, at the z-coordinate corresponding to the largest electric field intensity. The waveguide's circular cross-section can be seen at the center of each map.

#9476 - $15.00 USD Received 15 November 2005; revised 5 November 2005; accepted 11 November 2005

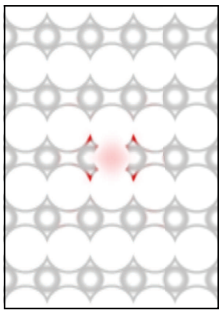

band 392, $z = \frac{\sqrt{2}}{4}a$

Fig. 6. Energy in the electric field for a mode at the Brillouin zone center for the 392^{th} band. The gray regions represent Ge. The structure is the same as in Fig. 4(b). Plotted here is the energy distribution on a plane perpendicular to the waveguide, located at $z = \frac{\sqrt{2}}{4}a$.

4. Chained spheres waveguide

In general, surface-like modes typically arise in an air defect when the interface cuts through regions in which the bulk modes in the band right below the gap has a large electric field intensity [22-24]. Therefore we examine the intensity profile of the mode associated with the 8^{th} band in the perfect crystal. For this mode, the high intensity regions are found around $(\frac{1}{2},0,\frac{1}{2})$ and $(0,\frac{1}{2},0)$ in our non-primitive lattice vectors basis. Therefore, in the case of a cylindrical air waveguide, it is difficult to avoid having the surface of the waveguide to cut through these high intensity regions. Instead of a cylindrical air waveguide, we consider an array of air spheres aligned along the $[1\overline{1}0]$ direction, with one sphere per non-primitive unit cell. The center of the sphere is located at $(\frac{1}{2},0,\frac{1}{2})$ in the basis $(\vec{a_1}',\vec{a_2}',\vec{a_3}')$, and coincides with the high intensity region of the bulk modes. Thus the center of the sphere lies in the plane $z = \sqrt{2}a/4$.

The corresponding dispersion relations are displayed in Fig. 7(a), (b) and (c) for air spheres of radius $R = 0.25a$, $R = 0.30a$ and $R = 0.45a$, respectively. We clearly observe that for this new defect geometry, the number of modes in the bandgap has decreased significantly. In particular, the band 392 has now a single intersection, with the band labelled 393.

Figures 8 and 9 refer to a structure containing air spheres of radius $R = 0.30a$. They show the intensity profile of the bandgap modes, at the Brillouin zone center. These results should be compared to those found with the cylindrical air waveguide of radius $R = 0.30a$ in Fig. 5. The 392^{th} and 393^{th} bands show very similar field patterns for these distinct defect geometries. The 394^{th} (395^{th}) band intensity distribution in Fig. 8 is analogous to the 395^{th} (394^{th}) band intensity distribution in Fig. 5. As in the case of a cylindrical waveguide, we observe that only the mode corresponding to the 392^{th} band possesses a significant fraction of energy in air. For a sphere radius of $R = 0.30a$, this band appears to be essentially flat over the whole Brillouin zone. The width of this band, however, is substantially increased when the air sphere radius is increased to $R = 0.45a$. As the periodicity in the $\Gamma - K$ direction is $\frac{\sqrt{2}a}{2}$, the defect is now an array of overlapping spheres. The calculation of the photonic bands for this structure, in Fig. 7(c), shows only two bands in the center of the gap. The 392^{th} band covers a wide range of frequencies (from 0.836 to 0.901 c/a), i.e. the same order of magnitude as the range covered with a cylindrical air waveguide of radius $R = 0.30a$ (see Fig. 4(b)). This can be understood by an examination of the electric field energy distribution in Fig. 10 and 11. The cross-section of

#9476 - $15.00 USD Received 15 November 2005; revised 5 November 2005; accepted 11 November 2005

the air sphere with the plane where the intensity is maximal (i.e. $z = 0$) has a radius

$$r = \sqrt{(0.45a)^2 - (\frac{\sqrt{2}a}{4})^2} = 0.28\,a, \tag{1}$$

very close to the radius $R = 0.30\,a$ of the cylindrical waveguide. This give rise to an identical intensity distribution for the 392^{th} band and the 393^{th} band of both structures.

Bands 392 and 393 have different polarization properties. The color plots in Fig. 12(a) and (b) represent the modulus of the electric field at the Brillouin zone center on the same plane as in Fig. 10 (i.e. $z = 0$), where the energy in the electric field is maximum. For the 392^{th} band, in Fig. 12(a), the electric fields are in the direction of the waveguide. By contrast, for the 393^{th} band, in Fig. 12(b), the electric fields are completely within the plane. A vector plot of the in-plane electric field is superimposed. As these two bands are associated to modes with different polarizations, they can be selectively coupled. For a correct polarization, band 392 can be considered as covering a broad "single-mode" region.

For band 392, in the case of a linear defect made of an array of air spheres of radius R, the defect band extends across the entire Brillouin zone, inside the bandgap and exhibit vanishing group velocity at both the center and edge of the Brillouin zone. We plot the waveguiding bandwidth for band 392 as a function of the air sphere radius R in Fig. 13. The waveguiding bandwidth reaches its maximum at $113nm$ centered at a wavelength of $1.5\mu m$ for a sphere radius $R = 0.45a = 0.58\mu m$. In that case, the air waveguide mode exhibits a band center group velocity of approximately $0.22c_0$, where c_0 is the velocity of light in vacuum. It should be noted that this maximal bandwidth is larger than the optimized single-mode bandwidth of $74nm$ predicted in a 2D-3D heterostructure, where a linear defect is written in a 2D PC layer embedded between two 3D photonic bandgap cladding layers of inverse opal structure [11]. In the 2D-3D heterostructure, the bandwidth is actually limited by the reduced gap size in the 2D layer. This is not the case in the present geometry.

Waveguides made of a sequence of coupled resonators have been studied in previous works with a formalism similar to the tight-binding method in solid-state physics [25]. In the periodic array of defects, the coupling of neighbouring defects creates a narrow band of states around the resonance frequency of the single defect. This model, giving rise to a dispersion relation that can be written as a cosine function, was demonstrated in a diamond structure when a linear chain of defects was introduced [26]. However, this theory assumes a weak coupling between the resonators and an interaction limited to the nearest neighbors, which is not the case for our waveguide made of an array of overlapping air spheres of radius $R = 0.45a$. Therefore our system cannot be properly described in terms of a tight-binding model. Instead, the strong coupling between the defects of the chain gives rise to a large bandwidth for the waveguiding mode.

#9476 - $15.00 USD Received 15 November 2005; revised 5 November 2005; accepted 11 November 2005

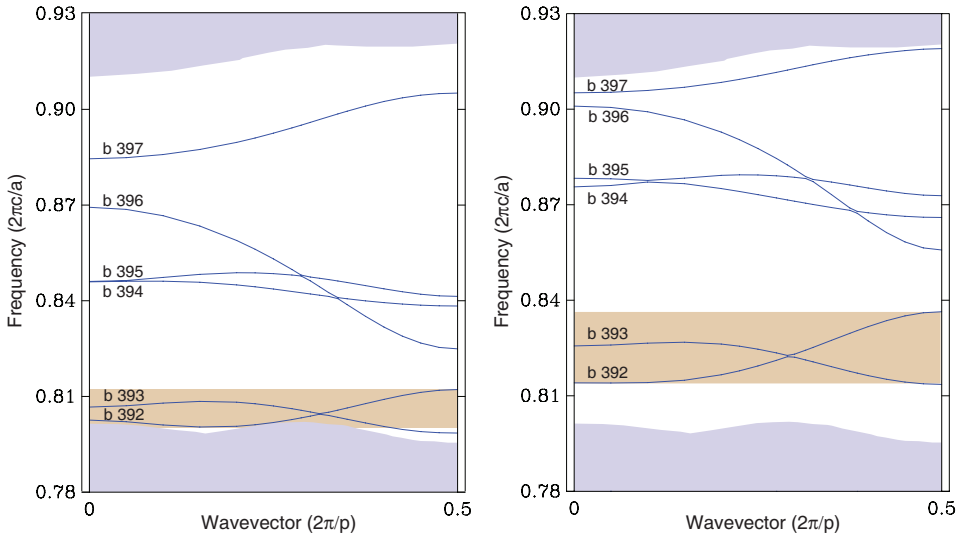

(a) $R = 0.25a$ (b) $R = 0.30a$

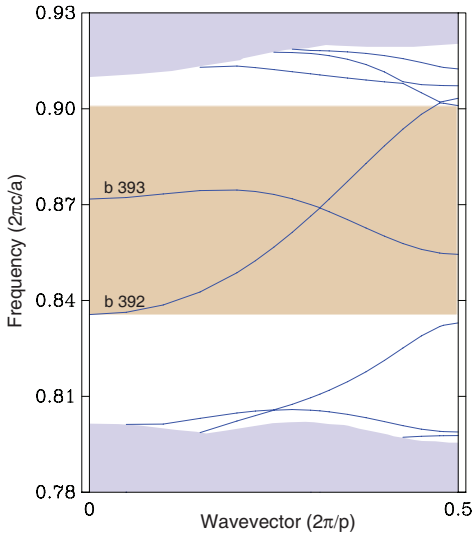

(c) $R = 0.45a$

Fig. 7. Projected band structure for the inverse opal photonic crystal with a linear defect made of an array of air spheres of radius R. The array is along the $[1\bar{1}0]$ direction. The periodicity p in this direction is $\frac{\sqrt{2}}{2}\,a$. The shaded blue areas indicate the propagating modes in the perfect three-dimensional photonic crystal. The brown area indicates the region covered by the band that possesses a significant fraction of energy in air.

#9476 - $15.00 USD Received 15 November 2005; revised 5 November 2005; accepted 11 November 2005

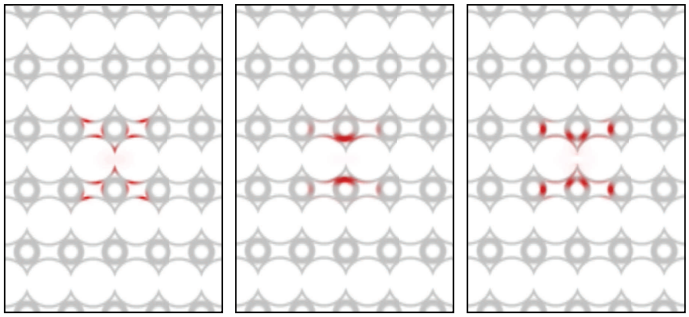

(a) band 392, $z = 0$ (b) band 393, $z = 0$ (c) band 394, $z = 0$

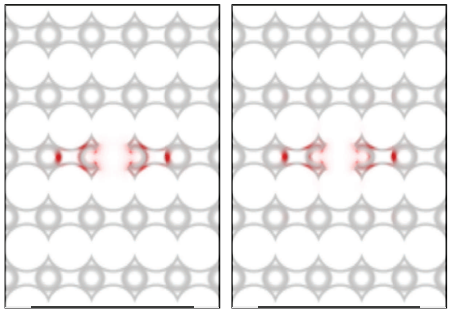

(d) band 395, $z = \frac{\sqrt{2}}{4}a$ (e) band 396, $z = \frac{\sqrt{2}}{4}a$

Fig. 8. Energy in the electric field for the modes at the Brillouin zone center, in the defect bands inside the bandgap. The gray regions represent Ge. The defect consists of an array of air spheres of radius $R = 0.30\,a$ along the $[1\bar{1}0]$ direction. For each of these bands, the plot describes the electric energy distribution on the plane perpendicular to the waveguide, at the z-coordinate corresponding to the largest electric field intensity. The center of one of these spheres can be seen at the center of the maps located at $z = \frac{\sqrt{2}}{4}a$.

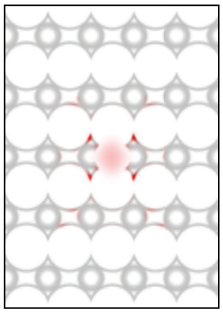

band 392, $z = \frac{\sqrt{2}}{4}a$

Fig. 9. Energy in the electric field for a mode at the Brillouin zone center for the 392^{th} band. The gray regions represent Ge. The structure is the same as in Fig. 7(b). Plotted here is the energy distribution on a plane perpendicular to the waveguide, located at $z = \frac{\sqrt{2}}{4}a$. The center of one of the air spheres constituting the line defect is located at the center of the plot.

#9476 - $15.00 USD Received 15 November 2005; revised 5 November 2005; accepted 11 November 2005

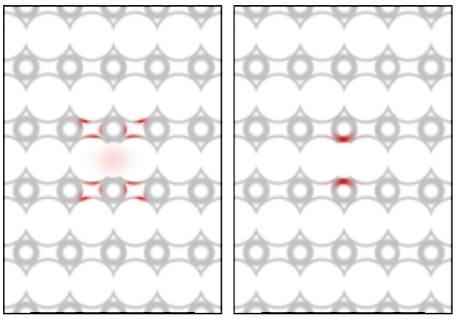

(a) band 392, $z = 0$ (b) band 393, $z = 0$

Fig. 10. Energy in the electric field for the modes at the Brillouin zone center, in the defect bands inside the bandgap. The gray regions represent Ge. The defect consists of an array of air spheres of radius $R = 0.45a$ along the $[1\bar{1}0]$ direction. For each of these bands, the plot describes the electric energy distribution on the plane perpendicular to the waveguide, at the z-coordinate corresponding to the largest electric field intensity. The center of one of these spheres can be seen at the center of the maps located at $z = \frac{\sqrt{2}}{4}a$.

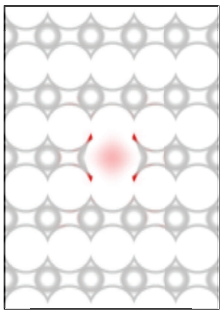

band 392, $z = \frac{\sqrt{2}}{4}a$

Fig. 11. Energy in the electric field for a mode at the Brillouin zone center for the 392^{th} band. The gray regions represent Ge. The structure is the same as in Fig. 7(c). Plotted here is the energy distribution on a plane perpendicular to the waveguide, located at $z = \frac{\sqrt{2}}{4}a$. The center of one of the air spheres constituting the line defect is located at the center of the plot.

#9476 - $15.00 USD Received 15 November 2005; revised 5 November 2005; accepted 11 November 2005

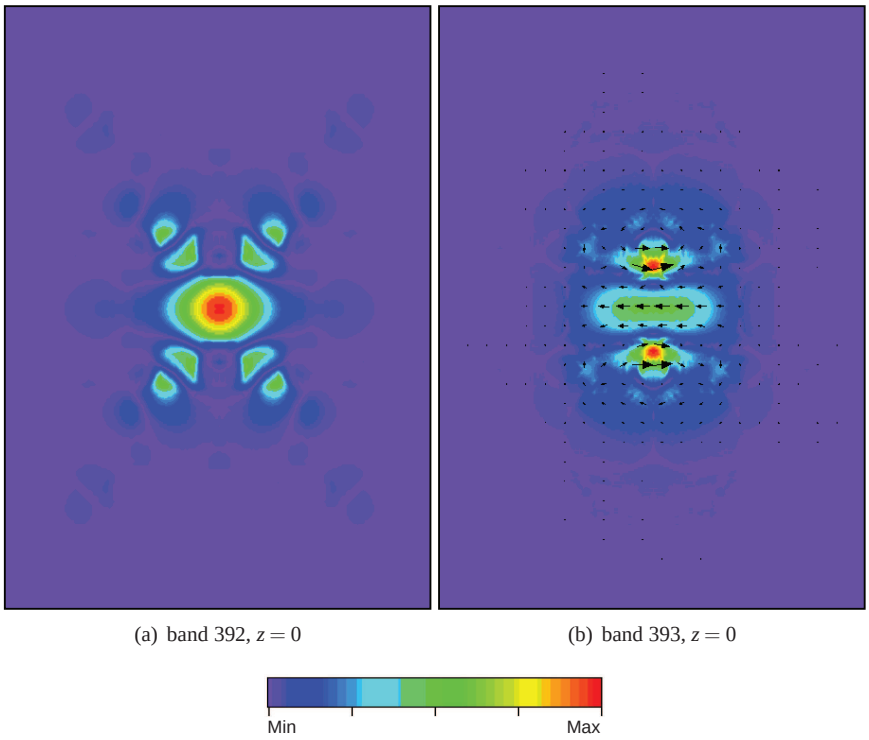

(a) band 392, $z = 0$ (b) band 393, $z = 0$

Fig. 12. Electric field patterns of the defect modes at the Brillouin zone center. The color plots correspond to $|\overline{E}|$ on the same plane $z = 0$ as in Fig. 10, in an inverted opal structure in which an array of air spheres of radius $R = 0.45a$ has been drilled along the $[1\bar{1}0]$ direction. (a) Band 392. The electric fields are completely perpendicular to the plane, i.e. they lie in the direction of the waveguide. (b) Band 393. The electric fields are completely within the plane. A vector plot of the in-plane electric field is superimposed.

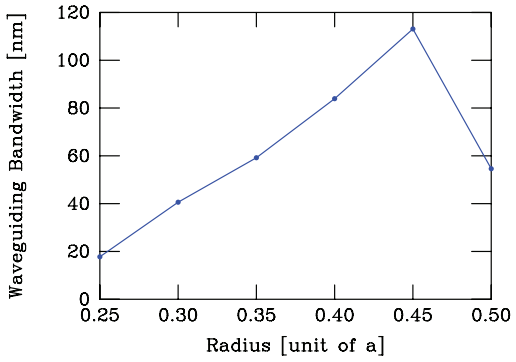

Fig. 13. Waveguiding bandwidth as a function of air sphere radius, for a defect guide consisting of an array of air spheres along the $[1\bar{1}0]$ direction in the inverse opal structure. Considered here is band 392, centered at a wavelength of $1.5\mu m$.

#9476 - $15.00 USD Received 15 November 2005; revised 5 November 2005; accepted 11 November 2005

5. Conclusion

In this work, we have reported a theoretical analysis on line defects in self-assembled photonic crystals. Several defect geometries have been considered in order to achieve a structure with a large single-mode bandwidth. Most of these geometries, and in particular the cylindrical air waveguides, have been shown to give rise to a large number of surface-like states in the bandgap. These surface-like modes are inappropriate for optical circuit integration. In order to avoid these states, the geometry of the line defect has been altered. It has been shown that a linear chain of defect air spheres in the inverse opal structure gave rise to only two modes of different polarizations at the center frequency of the bandgap. The structure has been optimized in order to obtain the maximal waveguiding bandwidth of $113nm$ centered at a wavelength of $1.5\mu m$.

It is known that the complete gap in inverted opal structures can be quite susceptible to disorders [27]. Nevertheless, this band gap has already been very clearly observed in high-quality experimental structures [18]. In this design, a significant portion of the waveguide dispersion curve lies at the center of the gap, which is less susceptible to disorder effects compared with gap edges.

The proposed structure is potentially amenable to fabrication techniques like multi-photon polymerisation. Indeed, in our waveguide geometry where the single mode bandwidth is optimized, the air spheres diameter is approximately $1.16\mu m$, which is larger than the wavelength of $780nm$ at which the pulsed laser used in the multi-polymerisation process is operating [20].

In crystalline Ge, the imaginary part of the refractive index is 5.67×10^{-3}. That translates in a propagation distance of approximately $50\mu m$. In the photonic crystal structure, a significant portion of the power is in air so that the propagation distance could be significantly longer compared with Ge. The design principle should be applicable to Si inverted opals as well.

Acknowledgments

The work was supported in part by Department of Defense Multidisciplinary University Research Initiative (ARO-MURI) grant DAAD19-03-1-0227. The simulations were performed through the support of a National Science Foundation National Resource Allocation Committee (NSF-NRAC) program. V.L. was supported as Postdoctoral Fellow by the Belgian National Fund for Scientific Research (FNRS). We acknowledge fruitful discussions with Stephanie Pruzinsky and Prof. Paul Braun.

#9476 - $15.00 USD Received 15 November 2005; revised 5 November 2005; accepted 11 November 2005